Generation of four-partite Greenberger-Horne-Zeilinger and *W* states by using a high-finesse bimodal cavity

D. Gonţa,[1,*] S. Fritzsche,[1,2,†] and T. Radtke[3,‡]
[1]*Max-Planck-Institut für Kernphysik, Postfach 103980, D-69029 Heidelberg, Germany*
[2]*Gesellschaft für Schwerionenforschung, D-64291 Darmstadt, Germany*
[3]*Institut für Physik, Universität Kassel, Heinrich-Plett-Strasse 40, D-34132 Kassel, Germany*
(Received 14 February 2008; published 9 June 2008)

We propose two schemes to engineer four-partite entangled Greenberger-Horne-Zeilinger (GHZ) and *W* states in a deterministic way by using chains of (two-level) Rydberg atoms within the framework of cavity QED. These schemes are based on the resonant interaction of the atoms with a bimodal cavity that simultaneously supports, in contrast to a single-mode cavity, two independent modes of the photon field. In addition, we suggest the schemes to reveal the nonclassical correlations for the engineered GHZ and *W* states. It is shown how these schemes can be extended in order to produce general *N*-partite entangled GHZ and *W* states.

DOI: 10.1103/PhysRevA.77.062312 PACS number(s): 42.50.Pq, 42.50.Dv, 03.67.Mn

I. INTRODUCTION

Entanglement is known today as a key feature of quantum mechanics; it has been found important not only for studying the nonlocal and nonclassical behavior of quantum particles but also for applications in quantum engineering and quantum-information theory [1], such as super-dense coding [2], quantum cryptography [3], or for the quantum search algorithms [4]. Apart from the Bell states as a prototype of two-partite entangled states, several attempts have been made recently in order to create and control entanglement also for more complex states. Owing to the fragile nature of most of these states, however, their manipulation still remains a challenge for experiment and only a few proof-of-principle implementations have been realized so far that generate entangled states with more than two parties in a well-defined way. For systems of three parties, for example, one often considers the Greenberger-Horne-Zeilinger (GHZ) state [5]

$$|\Psi^{(3)}_{\mathrm{GHZ}}\rangle = \frac{1}{\sqrt{2}}(|\uparrow_1,\uparrow_2,\uparrow_3\rangle + |\downarrow_1,\downarrow_2,\downarrow_3\rangle) \tag{1}$$

and the *W* state [6]

$$|\Phi^{(3)}_{W}\rangle = \frac{1}{\sqrt{3}}(|\uparrow_1,\downarrow_2,\downarrow_3\rangle + |\downarrow_1,\uparrow_2,\downarrow_3\rangle + |\downarrow_1,\downarrow_2,\uparrow_3\rangle) \tag{2}$$

as two kinds of pure entangled three-qubit states. In this notation, as usual, $|\uparrow_n\rangle$ and $|\downarrow_n\rangle$ refer to the two distinguishable projections of qubit n, such as its spin, excitation state, polarization or some other two-level property of a given quantum system, while $|\uparrow_1,\ldots,\uparrow_n\rangle$ denotes the direct product of states $|\uparrow_1\rangle,\ldots,|\uparrow_n\rangle$, respectively. The GHZ and *W* states are known also as genuine entangled states since they cannot be transformed into each other under local operations and classical communication (LOCC) protocols. Indeed, the properties of these states have been explored in details during recent years with regard to different quantum measures, separability criteria, or concerning the violation of local realism [7,8]. For instance, while the GHZ state is fragile under qubit loss, leading to a separable quantum state if just one of the three qubits is traced out, the three-partite *W* state still results in the Bell state $\frac{1}{\sqrt{2}}(|\uparrow_1,\downarrow_2\rangle+|\downarrow_1,\uparrow_2\rangle)$ when the third qubit is projected upon the state $|\downarrow_3\rangle$. Various experiments have been reported in the literature for generating three-qubit GHZ and *W* states by applying optical systems [9,10], nuclear magnetic resonance [11,12], cavity QED [13,14], or ion trapping techniques [15].

In the framework of cavity QED in particular, in which neutral atoms couple to a high-finesse microwave cavity, Rauschenbeutel and co-workers [13] prepared the excited states of three two-level Rydberg atoms (using circular atomic states which correspond to levels n and $n+1$) in an entangled GHZ state (1) by utilizing a single-mode superconducting cavity [16,17]. In these experiments, the cavity field mediates the interactions between the atoms that pass successively through the cavity, and the control over the light fields and atoms (atomic chain) is achieved owing to the high quality of the cavity. In the language of these cavity experiments, usually two parts of the measurements are distinguished: The (so-called) longitudinal experiment to prepare the entangled state of the Rydberg atoms, and the transversal experiment that helps to reveal the produced entanglement. This latter part is realized by observing the nonclassical correlations for a series of projective measurements on the population of the Rydberg states after the given chain of atoms has passed through the cavity and the atomic Ramsey interferometer (see Sec. III). The experiments by Rauschenbeutel *et al.* nicely demonstrated the possibility of using an atom-cavity (quantum) phase gate in order to entangle three atomic qubits, and it has triggered the community to undertake steps toward the controlled manipulation of multipartite entangled states. Up to the present, however, only a few case studies are known [18–20], where the four-partite entangled states have been generated by using optical systems and ion trapping techniques.

Of course, a detailed analysis is required for every particular realization of *N*-partite quantum systems in order to

*gonta@physi.uni-heidelberg.de
†s.fritzsche@gsi.de
‡tradtke@physik.uni-kassel.de

work out an experimental scheme that enables one to generate and observe reliably entanglement in the system. From the viewpoint of theory, such a scheme can be understood also as a quantum circuit or, simply, a (temporal) sequence of steps for dealing with the individual parts (qubits) of the system. In the present work, we suggest two (experimentally feasible) schemes for generating the four-partite GHZ and W states

$$|\Psi_{\mathrm{GHZ}}^{(4)}\rangle = \frac{1}{\sqrt{2}}(|\uparrow_1,\uparrow_2,\uparrow_3,\uparrow_4\rangle + |\downarrow_1,\downarrow_2,\downarrow_3,\downarrow_4\rangle), \tag{3}$$

$$|\Phi_W^{(4)}\rangle = \frac{1}{2}(|\uparrow_1,\downarrow_2,\downarrow_3,\downarrow_4\rangle + |\downarrow_1,\uparrow_2,\downarrow_3,\downarrow_4\rangle + |\downarrow_1,\downarrow_2,\uparrow_3,\downarrow_4\rangle + |\downarrow_1,\downarrow_2,\downarrow_3,\uparrow_4\rangle) \tag{4}$$

in a deterministic way within the framework of cavity QED. The proposed schemes are based on a bimodal cavity which, in contrast to single-mode cavities, contains two independent cavity modes (of the light field). Below, we describe the individual steps of how the atoms need to interact with either the first or the second cavity mode, and a graphical language is utilized in order to display these steps in terms of a quantum circuit. A resonant strong-coupling regime is assumed, in which the dissipation of the light field in the cavity is negligible in the course of interaction. After completion of these steps (the longitudinal experiment), an entangled GHZ or W state is produced for a chain of four (two-level) atoms that have passed through the cavity. In practice, however, the final state of the atoms might not be pure but rather a statistical mixture of states due to decoherence and other imperfections in a given experiment. To understand the final state that is obtained for the atomic chain, we also suggest—as the transversal part of the measurements—a scheme for analyzing its nonclassical correlations, i.e., to provide a proof that (or to which extent) a four-partite GHZ and W state was generated indeed. The goal is to suggest a scheme that is well adapted to the recent developments in cavity QED [21] and, in particular, to the forthcoming generation of high-finesse microwave cavities that was announced recently [22] from the Laboratoire Kastler Brossel (ENS). In addition, we also show how the scheme below can be generalized quite easily to produce entangled GHZ and W states for any chain of N two-level Rydberg atoms.

The paper is organized as follows. In the next section, we briefly recall how the resonant interaction of a two-level Rydberg atom with a given mode of a cavity is described by the Jaynes-Cummings Hamiltonian, both for single and bimodal cavities. In Sec. IIA, we then present and explain the steps for generating with a chain of (four) atoms a four-partite GHZ state, and in Sec. II B those for a W state. For both states, the overall time evolution of the atoms-cavity system is displayed also in terms of quantum circuits. These steps are generalized in Sec. II C for N-partite states, i.e., any number of Rydberg atoms in the chain. In Sec. III, later, possible setups are discussed for performing transversal measurements in order to reveal the nonclassical correlations within the entangled atom chains. Finally, our conclusions are given in Sec. IV.

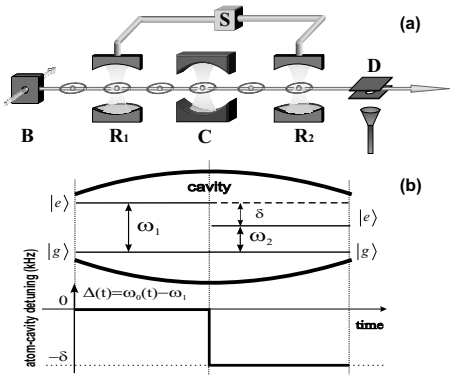

FIG. 1. (a) Schematic setup of the microwave cavity experiments in which a chain of Rydberg atoms from a source B passes through a Ramsey zone R_1, a superconducting cavity C, and the (second) Ramsey zone R_2 before the atoms are field ionized at the detector D. The classical field in the Ramsey zones is generated by a microwave source S. (b) Temporal matching of the $e \leftrightarrow g$ atomic transition frequency (ω_0) to the frequency ω_1 of the first cavity mode and the frequency ω_2 of the second mode in the course of the resonant atomic-cavity interaction. Apart from the matching of the atomic frequency (upper half), the lower part of this figure displays the time dependence of the atom-cavity detuning $\Delta(t)=\omega_0(t)-\omega_1$, implying a stepwise change from the resonant $A-C_1$ interaction regime to the resonant $A-C_2$ regime. See text for further discussions.

II. ENGINEERING OF ENTANGLED STATES BY USING BIMODAL CAVITIES

The resonant atom-cavity interaction regime is perhaps the simplest way to entangle in a controlled manner the atomic circular states and the quantized cavity field states with each other. For a sufficiently high quality (factor) of the cavity mirrors, this regime implies a strong atom-field coupling for which the dissipation of field energy in the course of the atom-cavity interaction becomes negligible. Indeed, avoiding the dissipation of the cavity field is crucial for engineering multipartite entangled states of atomic and/or photonic qubits in a deterministic way. Besides the quality of the cavity, the correct matching of the atomic frequency to the frequency of cavity mode (the so-called detuning) is also important in order to achieve a resonant interaction regime.

In the following, let us adopt the language of Haroche and co-workers for describing cavity QED experiments and to specify the circular states of the atoms and the state of the cavity. In their experiments, rubidium atoms are prepared to occupy one of the three (circular) levels with principal quantum numbers 51, 50, and 49 to which they are referred to as exited state $|e\rangle$, ground state $|g\rangle$, and state $|i\rangle$, respectively. Owing to the design of the microwave cavity, however, only the states $|e\rangle$ and $|g\rangle$ can be involved in the atom-cavity interaction because only the $e \leftrightarrow g$ transition frequency of the Rydberg atoms can be tuned to the frequency of the cavity mode(s). The classical field from the microwave source S [see Fig. 1(a)], in contrast, can be adopted to drive either the $e \leftrightarrow g$ or $g \leftrightarrow i$ transitions and is utilized for generating superpositions between these states.

The (time) evolution of an atom with a single-mode cavity is described, both for a resonant and nonresonant interac-

tion, by the Jaynes-Cummings Hamiltonian [23] ($\hbar=1$),

$$H=\omega_0 S_z+\frac{\Omega}{2}(S_+a_1+a_1^+S_-)+\omega_1\left(a_1^+a_1+\frac{1}{2}\right), \tag{5}$$

where ω_0 is the atomic $e\leftrightarrow g$ transition frequency, ω_1 is the frequency of the cavity field, and Ω is the atom-field coupling frequency. In this Hamiltonian, moreover, a_1 and a_1^+ denote the annihilation and creation operators for a photon in the cavity, which act upon the Fock states $|n\rangle$, while S_- and S_+ are the atomic spin lowering and raising operators that act upon the states $|e\rangle$ and $|g\rangle$, where the atomic states $|e\rangle$ and $|g\rangle$ are treated as the eigenstates of the spin operator S_z with eigenvalues $+1/2$ and $-1/2$, respectively. If there is not more than one photon in the cavity, then the overall atom-field state evolves during the resonant atom-cavity interaction, e.g., for a zero detuning ($0=\omega_0-\omega_1$), as

$$|e,0\rangle\rightarrow\cos(\Omega t/2)|e,0\rangle+\sin(\Omega t/2)|g,1\rangle, \tag{6a}$$

$$|g,1\rangle\rightarrow\cos(\Omega t/2)|g,1\rangle-\sin(\Omega t/2)|e,0\rangle, \tag{6b}$$

i.e., with a time evolution that is known also as Rabi rotation. In this rotation, t is the effective atom-cavity interaction time in the laboratory, Ωt is the respective angle, and a coupling constant $\Omega/2\pi=47$ kHz has been utilized in various microwave cavity QED experiments. Note that neither the state $|e,1\rangle$ nor $|g,0\rangle$ appears in the time evolution (6a) and (6b) in line with our physical intuition that the photon energy is stored either by the atom or the cavity but cannot occur twice in the system.

In order to minimize the contribution of thermal photons, which occur in microwave cavities due to thermal field leaks, the cavity is cooled down to 0.6 K in the experiments by Haroche and co-workers. Moreover, at the beginning of each experimental sequence the thermal photons are further minimized by sending an atom in its ground state through the cavity so that it interacts with a cavity mode for a π Rabi rotation and thus absorbs the remaining thermal photons from the cavity mode. By making use of both, such cooling and erasing techniques, an average number of $n_{\mathrm{th}}\simeq 0.02$ thermal photons has been achieved so far. This ensures that the destructive contribution of thermal photons on the evolution of cavity states during the main experimental sequence can be neglected.

In contrast to single-mode cavities, a bimodal cavity supports two independent and nondegenerate modes of light with different (orthogonal) polarization. Since the frequencies of these light modes are fixed by the geometry of the cavity, the atomic $e\leftrightarrow g$ frequency needs to be tuned in order that the atom interacts resonantly with either the first or the second field mode. In the language of quantum information, the additional cavity mode gives rise to another photonic qubit that may interact independently with the atomic qubits that pass through the cavity. Indeed, the design and development of bimodal cavities has been found to be an important step toward the coherent manipulation of complex quantum states and for performing fundamental tests in quantum theory [24–31]. Below, we shall denote the cavity modes by C_1 and C_2 and suppose that they are associated with the frequencies ω_1 and ω_2, such that $\omega_1-\omega_2\equiv\delta>0$. Owing to this fixed splitting in the frequency of the field modes, we refer to the detuning of the atomic frequency with regard to the cavity modes briefly as atom-cavity detuning. For the cavity utilized in the experiment by Rauschenbeutel and coworkers [24], especially a frequency splitting of $\delta/2\pi=128.3$ KHz was realized.

An entanglement of a Rydberg atom with the photon field of the cavity is achieved by tuning the $e\leftrightarrow g$ transition frequency as a function of time from being in resonance with one or the other cavity mode, while the atom passes through the cavity. For a proper detuning $\Delta(t)$ of the atomic frequency, a resonant interaction (regime) is then realized and can be switched between the two field modes. As seen from the lower part of Fig. 1(b), the atom is in resonance with the cavity mode C_1 for $\Delta(t)=0$ and with C_2 for $\Delta(t)=-\delta$, where a stepwise change from the $A-C_1$ to the $A-C_2$ resonant interaction is required. In practice, however, this stepwise change in the detuning $\Delta(t)$ is experimentally not feasible. In the experiments by Haroche and co-workers, the detuning is changed by applying a well-adjusted time-varying electric field across the gap between the cavity mirrors, so that the required (Stark) shift of the atomic transition frequency $\omega_0(t)$ is achieved. Instead of a sharp stepwise change of the atom-cavity detuning, therefore a rather smooth switch is produced within a finite time $\tau\simeq 1$ μs that corresponds to a $\frac{\pi}{10}$ angle in units of Rabi rotations. For a typical atom-cavity interaction time, this finite switch is not negligible and does affect the evolution of the cavity states [32]. In this paper, however, we shall not consider the effects of this finite switch, but shall assume a stepwise change in the detuning as indicated in the lower part of Fig. 1(b). From the experimental viewpoint, further improvements of the time-varying electric field characteristics are needed in order to produce a sufficiently short (and thus negligible) switching time from the $A-C_1$ to the $A-C_2$ resonant interaction.

We also note that, if the atom is tuned into resonance with one of the cavity modes, the second mode is frozen out from the atom-cavity interaction owing to the (large) splitting δ between the two cavity modes. Therefore, the overall $A-C_1-C_2$ time evolution of the atom-cavity state can be safely separated into two independent parts: The evolution due to the $A-C_1$ resonant interaction and that due to $A-C_2$. In practice, however, the splitting between the two cavity modes frequencies is often not large enough (for example, $\delta\approx 3$ Ω in the experiment of Rauschenbeutel and coworkers), and then neither one of the two cavity modes can be frozen out completely. This leads to a simultaneous interaction of the atom with both cavity modes and yields an effective mode wave mixing in the cavity [32]. Again, we shall not consider the simultaneous interaction with both cavity modes in this paper but assume the shift δ to be sufficiently large, so that the atom-cavity state evolves according to Eq. (6) during the $A-C_1$ interaction, and according to

$$|e,\bar{0}\rangle\rightarrow e^{i\delta\Omega t/2}[\cos(\Omega t/2)|e,\bar{0}\rangle+i\sin(\Omega t/2)|g,\bar{1}\rangle], \tag{7a}$$

$$|g,\bar{1}\rangle\rightarrow e^{i\delta\Omega t/2}[\cos(\Omega t/2)|g,\bar{1}\rangle+i\sin(\Omega t/2)|e,\bar{0}\rangle], \tag{7b}$$

during the $A-C_2$ interaction (period). In the evolution Eq. (7), the states $|\bar{0}\rangle$ and $|\bar{1}\rangle$ hereby refer to the Fock states of

the cavity mode C_2, and the phase factor $e^{i\delta\Omega t/2}$ arises from the energy difference $\hbar\delta$ between the two cavity modes being accumulated in the course of the Rabi rotation Ωt.

With this short reminder on the Jaynes-Cummings Hamiltonian and the (atom-cavity) interactions in a bimodal cavity, we are now prepared to present the steps that are necessary in order to generate four-partite entangled states for a chain of Rydberg atoms.

A. Four-partite GHZ state

Let us first consider the four-partite GHZ state (3) and assume that, initially, the cavity is empty, i.e., being in the state $|0,\bar{0}\rangle \equiv |0\rangle \times |\bar{0}\rangle$. Then, by using an auxiliary (Rydberg) source atom A_s in the excited state $|e\rangle$, we can prepare the cavity in a superposition of the two cavity modes

$$|\Psi_1\rangle = \frac{1}{\sqrt{2}}(ie^{i\delta\pi/\Omega}|0,\bar{1}\rangle + |1,\bar{0}\rangle). \tag{8}$$

According to our discussions above, this is achieved if the source atom first interacts with the mode C_1 ($\Delta=0$) for a Rabi rotation $\Omega t_0=\pi/2$, and afterwards with the cavity mode C_2 ($\Delta=-\delta$) for the rotation $\Omega t_1=\pi$. Owing to the rotations of the atom-cavity state in Eq. (6), we shall briefly refer to these interactions as Rabi $\pi/2$, respectively, π pulse, and display them in the figures by means of black diamonds with the rotation angle indicated inside. For a resonant interaction, of course, the subsequent application of these two rotations in Eqs. (6) and (7) with regard to the field modes C_1 and C_2 leads to a factorization of the source atom in its ground state $|g\rangle$, and that is therefore omitted from our further discussion (for further details, see the paper by Rauschenbeutel *et al.*, where this two-step sequence has been demonstrated also experimentally). For the sake of brevity, moreover, we shall not display explicitly the values Δ for the detuning of the atomic frequency which can easily be read off from the cavity modes as involved in some particular step of the resonant interaction.

In addition to the resonant atom-cavity interaction, we need to consider also the interaction of the Rydberg atoms with a (classical) microwave field that gives rise to a (coherent) superposition of atomic states before or after they pass through the cavity, and in dependence of the microwave pulse duration and its frequency (which can be tuned to the $e\leftrightarrow g$ or $g\leftrightarrow i$ atomic transitions). In the literature, such an interaction with a classical field is often called a Ramsey pulse and is denoted in the figures with gray circles, showing the interaction time in units of Ramsey rotations. In addition, we shall associate the letters R_1 or R_2 to these circles in order to denote the Ramsey zone in front or behind the cavity, see Fig. 1(a).

To generate a GHZ state for a chain of Rydberg atoms, being initially in the ground states $|g\rangle$, we can proceed as follows. If the cavity is in the superposition (8), the state of atom A_1 is first transformed just before it enters the cavity to

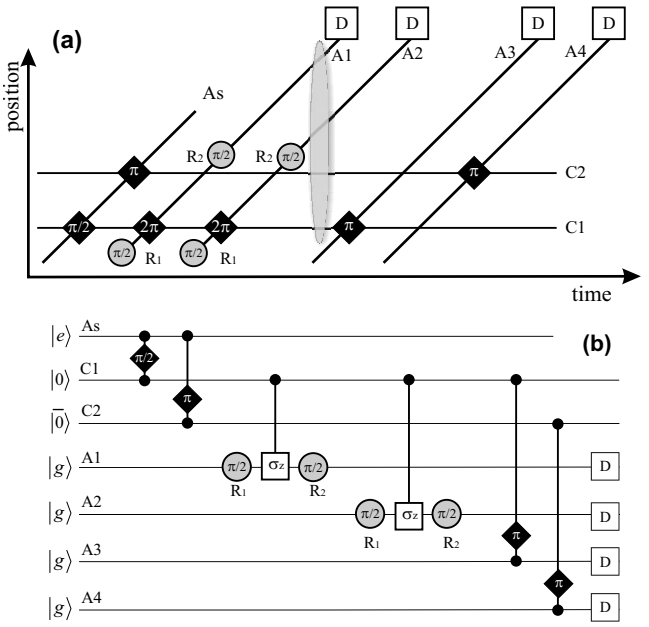

FIG. 2. (a) Temporal sequence for generating a four-partite GHZ state associated with the chain of Rydberg atoms A_1, A_2, A_3, and A_4. The pictograms in this figures are described in the text. The gray shadowed ellipse denotes the time when the entanglement of four qubits, the two photonic qubits C_1, C_2 and the two atomic qubits A_1, A_2 is achieved. (b) The corresponding quantum circuit in which the (four) Rydberg atoms are represented by the four lower lines, being initially prepared in the ground state $|g\rangle$, while the source atom A_s is shown as the uppermost line.

$$|g_1\rangle \to \frac{1}{\sqrt{2}}(|i_1\rangle + |g_1\rangle). \tag{9}$$

This is achieved by using a $\pi/2$ Ramsey pulse tuned to the $g\leftrightarrow i$ transition frequency while the atom A_1 crosses the first zone R_1. For the sake of brevity, we shall denote these interactions by $R_1(\pi/2,\omega_{g\leftrightarrow i})$, with ω_* being the frequency of the microwave source S. After the atom A_1 has left the Ramsey zone, it enters the cavity and interacts with mode C_1 for a Rabi rotation $\Omega t_3=2\pi$. The overall atom-cavity state then becomes

$$|\Psi_3\rangle = \frac{1}{2}[ie^{i\delta 3\pi/\Omega}|(g_1+i_1),0,\bar{1}\rangle - |(g_1-i_1),1,\bar{0}\rangle]. \tag{10}$$

The effect of this 2π rotation can be seen easily from Eq. (6) which implies that the transformation $|e_1,0\rangle \to -|e_1,0\rangle$ and $|g_1,1\rangle \to -|g_1,1\rangle$, is made. Of course, this transformation just describes a $\sigma_z=2S_z$ quantum (logic) gate that is applied to the atom-cavity system. After the atom has passed through the cavity, it is subjected again to a $R_2(\pi/2,\omega_{g\leftrightarrow i})$ pulse inside the second Ramsey zone [see Fig. 2(a)], thus leading to the state

$$|\Psi_4\rangle = \frac{1}{\sqrt{2}}(ie^{i\delta 3\pi/\Omega}|i_1,0,\bar{1}\rangle - |g_1,1,\bar{0}\rangle), \tag{11}$$

and where the unitary transformation [cf. (9)]

$$|g\rangle \to \frac{1}{\sqrt{2}}(|i\rangle + |g\rangle), \quad |i\rangle \to \frac{1}{\sqrt{2}}(|i\rangle - |g\rangle) \tag{12}$$

has been utilized. A more detailed discussion of these (three) steps was given in Rauschenbeutel *et al.*, where this sequence of Ramsey and Rabi pulses was demonstrated also experimentally for the first time. After the atom A_1, the second atom A_2 from the chain undergoes the same temporal sequence of interactions. Leaving apart the details, these transformations result in the state

$$|\Psi_7\rangle = \frac{1}{\sqrt{2}}(ie^{i\delta 5\pi/\Omega}|i_1,i_2,0,\bar{1}\rangle + |g_1,g_2,1,\bar{0}\rangle), \tag{13}$$

after the second atom has left the setup. Let us note that already now we have generated a four-partite GHZ-type state for the two atoms A_1 and A_2 as well as the two cavity modes C_1 and C_2, respectively. For the atoms, moreover, only the two neighbor states $|i\rangle$ and $|g\rangle$ are involved in the expression (13). In order to generate the GHZ state for a chain of four atoms, we need to map the information of the photonic qubits upon the Rydberg atoms A_3 and A_4. This is done quite easily if the atom A_3 interacts with the mode C_1 for $\Omega t_8 = \pi$ and atom A_4 with the mode C_2 for $\Omega t_9 = \pi$. Using Eqs. (6) and (7), we then see that the cavity states $|0\rangle$ and $|\bar{0}\rangle$ are mapped upon the ground states $|g_3\rangle$ and $|g_4\rangle$ of the two atoms, while $|1\rangle$ and $|\bar{1}\rangle$ are mapped upon the exited states $|e_3\rangle$ and $|e_4\rangle$, respectively. For these reasons, the overall atom-cavity state (13) is mapped upon the four Rydberg atom state

$$|\Psi^{(4)}_{\mathrm{GHZ}}\rangle = \frac{1}{\sqrt{2}}(e^{i\psi}|i_1,i_2,g_3,e_4\rangle + |g_1,g_2,e_3,g_4\rangle), \tag{14}$$

whereas the cavity state is factorized out in the vacuum state $|0,\bar{0}\rangle$. Obviously, the state (14) is equivalent to the state (3) under the change of notation [33]

$$|\downarrow_1\rangle = |i_1\rangle, \quad |\uparrow_1\rangle = |g_1\rangle, \quad |\downarrow_2\rangle = |i_2\rangle, \quad |\uparrow_2\rangle = |g_2\rangle, \tag{15a}$$

$$|\downarrow_3\rangle = |g_3\rangle, \quad |\uparrow_3\rangle = |e_3\rangle, \quad |\downarrow_4\rangle = |e_4\rangle, \quad |\uparrow_4\rangle = |g_4\rangle, \tag{15b}$$

except for the factor $e^{i\psi}$, with $\psi = \frac{7\pi}{\Omega}\delta$, that has no effect on the final-state probability to find the wave packet of atomic chain $A_1 - A_4$ in either the state $|i_1,i_2,g_2,e_4\rangle$ or $|g_1,g_2,e_4,g_4\rangle$. These probabilities are measured by the detectors, which are indicated in the figures by the capital D (within a box).

Besides displaying the individual interactions between the atoms and cavity, that is the particular sequence of Ramsey and Rabi pulses, a quantum circuit representation of the overall (unitary) transformation is shown in Fig. 2(b). Of course, both representations (a) and (b) in Fig. 2 are equivalent and can be utilized on purpose, where the latter one can be easily translated into quantum gates. Instead of the 2π Rabi rotation, the equivalent σ_z gate and the initial state of all (atomic and photonic) qubits are then shown explicitly. This compact notation for describing the unitary evolution of the atom-field system in the framework of cavity QED has been introduced originally by Haroche and co-workers and has been adopted here for the present discussion.

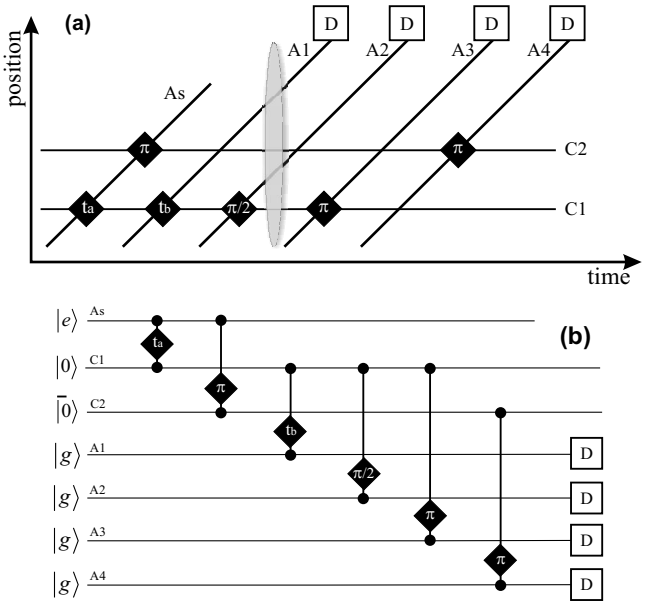

FIG. 3. (a) Temporal sequence for generating a four-partite W state associated with the chain of Rydberg atoms A_1, A_2, A_3, and A_4. Again, the gray shadowed ellipse denotes the time when the entanglement of four qubits, the two photonic qubits C_1, C_2 and the two atomic qubits A_1, A_2 is achieved. (b) The corresponding quantum circuit in which the (four) Rydberg atoms are represented by the four lower lines.

B. Four-partite W state

A similar pulse sequence as above for the GHZ state can be worked out in order to generate a four-partite W state (4) for a chain of (four) Rydberg atoms; this pulse sequences can be expressed again either as temporal sequence for the passage of atoms through the Ramsey zones and cavity [Fig. 3(a)] or as quantum circuit [Fig. 3(b)]. Unlike the generation of the state (8), however, here we initially prepare the two field modes of the cavity in the superposition

$$|\Phi_1\rangle = \frac{1}{2}(ie^{i\delta\pi/\Omega}|0,\bar{1}\rangle + \sqrt{3}|1,\bar{0}\rangle) \tag{16}$$

by using the source atom A_s in the exited state $|e\rangle$ and by interacting first with mode C_1 for a Rabi rotation $\Omega t_0 = 2\arccos(\frac{1}{2})$ and subsequently with mode C_2 for $\Omega t_1 = \pi$. Applying Eqs. (6) and (7), we see that these pulses result in the cavity state (16), while the source atom is factorized out in its ground state.

Next, the Rydberg atoms A_1 and A_2 pass through the cavity, being initially in the ground state. We let A_1 interact with the mode C_1 for a Rabi rotation $\Omega t_2 = 2\arccos(\sqrt{\frac{2}{3}})$, and A_2 with C_1 for $\Omega t_3 = \pi/2$. Then, the overall atom-cavity state is given by

$$|\Phi_3\rangle = \frac{1}{2}(ie^{i\delta(3\pi/2\Omega+t_2)}|g_1,g_2,0,\bar{1}\rangle + |g_1,g_2,1,\bar{0}\rangle - |g_1,e_2,0,\bar{0}\rangle - |e_1,g_2,0,\bar{0}\rangle), \tag{17}$$

i.e., by a W-type entangled state between the two photonic qubits C_1, C_2 and the atomic qubits A_1, A_2. To map the information of the photonic qubits upon the Rydberg atoms A_3 and A_4, a very similar procedure can be applied as for the GHZ state in Sec. II A: The atom A_3 first interacts with mode C_1 for a Rabi rotation $\Omega t_4 = \pi$ before A_4 enters the cavity and does the same with C_2 for $\Omega t_5 = \pi$. If both atoms enter the cavity in their ground state, the overall state of the atom chain becomes

$$|\Phi_W^{(4)}\rangle = \frac{1}{2}(e^{i\phi}|g_1,g_2,g_3,e_4\rangle + |g_1,g_2,e_3,g_4\rangle + |g_1,e_2,g_3,g_4\rangle + |e_1,g_2,g_3,g_4\rangle), \tag{18}$$

while the cavity (state) is factorized out. The state (18) coincides with the state (4) under the change of notation

$$|\uparrow_1\rangle = |e_1\rangle, \quad |\downarrow_1\rangle = |g_1\rangle, \quad |\uparrow_2\rangle = |e_2\rangle, \quad |\downarrow_2\rangle = |g_2\rangle, \tag{19a}$$

$$|\uparrow_3\rangle = |e_3\rangle, \quad |\downarrow_3\rangle = |g_3\rangle, \quad |\uparrow_4\rangle = |e_4\rangle, \quad |\downarrow_4\rangle = |g_4\rangle, \tag{19b}$$

and where, again, the exponential factor $e^{i\phi}$ with $\phi = \delta(\frac{7\pi}{2\Omega} + t_2)$ does not affect the final-state probability to find the wave packet of atomic chain $A_1 - A_4$ in either the state $|g_1,g_2,g_3,e_4\rangle$, $|g_1,g_2,e_3,g_4\rangle$, $|g_1,e_2,g_3,g_4\rangle$, or $|e_1,g_2,g_3,g_4\rangle$, respectively.

C. Generation of N-partite states

In the experiments by Rauschenbeutel *et al.*, the generation of the three-partite GHZ state was reported with a fidelity of 0.54%. This rather low value of fidelity, that is just above of the threshold 1/2 necessary for proving the production of this entangled state, is caused mainly by the low surface quality of the cavity mirrors, i.e., the local roughness and the deviations from the spherical geometry, as well as by the leakage of the cavity field due to its interaction with the environment. Under the assumption of negligible dissipation, the quality factor that characterizes the surface quality of cavity mirrors, is then proportional to the (coherent) photon storage time and thus determines the number of quantum logical operations that can be executed successively before the atom-cavity state becomes completely destroyed. This rapid loss of coherence during the atom-cavity state evolution, has stimulated the group of Raimond and Haroche at Laboratoire Kastler Brossel (ENS) to develop a new generation of cavity devices that was announced recently. With this new and ultrahigh-finesse cavity, the quality factor was increased by about two orders of magnitude, in fact, a very remarkable improvement that may enable them to perform more than 100 quantum logical operations within the lifetime of the cavity field. Moreover, by utilizing the toroidal form of the cavity mirrors (instead of spherical ones as used previously), the modes frequency splitting δ was increased by about one order of magnitude. This large increase ensures that an atom is coupled to one single mode only and, thus, that the effective mode wave mixing in the cavity mentioned above becomes negligible. Owing to this recent success, it seems justified to suggest new experiments in which multipartite entangled states can be generated with a trustworthy fidelity.

To this end, let us consider the N-partite (extension to the) GHZ and W states

$$|\Psi_{\mathrm{GHZ}}^{(N)}\rangle = \frac{1}{\sqrt{2}}(|\uparrow_1,\ldots,\uparrow_N\rangle + |\downarrow_1,\ldots,\downarrow_N\rangle),$$

$$|\Phi_W^{(N)}\rangle = \frac{1}{\sqrt{N}}(\overbrace{|\uparrow_1,\downarrow_2,\ldots,\downarrow_N\rangle + \cdots + |\downarrow_1,\downarrow_2,\ldots,\uparrow_N\rangle}^{N\ \text{terms}}).$$

For these states, N-partite entanglement can be generated in a similar way as discussed above by applying the individual steps in Figs. 4(a) and 4(b). In this procedure, a fully entangled state is first generated for $N-2$ atoms and the cavity; then, the information from the cavity field modes are mapped upon two additional Rydberg atoms in order to obtain a GHZ or W state associated with the atom chain $A_1 - A_N$. The time intervals t_i to perform the individual Rabi rotations on the atom-cavity states [Fig. 4(b)] are given by

$$t_1 = \frac{2}{\Omega}\arccos\left(\frac{1}{\sqrt{N}}\right), \quad t_n = \frac{2}{\Omega}\arccos\left(\sqrt{\frac{N-n}{N-n+1}}\right)$$

with $n = 2,\ldots,N-1$. There is not much need to mention here about these operations since the individual steps can be easily recognized from Fig. 4 as well as from our discussion in Secs. II A and II B above.

Suppose one could implement the extensions above, the question that naturally arises is up to which N one may proceed in line of the recent developments in cavity QED. To estimate such a practical limit in the number of atoms N, let us consider the most time consuming scenario—the N-partite GHZ state, for which each additional atomic qubit is incorporated into the final entangled state for the price of a 2π Rabi rotation (σ_z gate). If we assume that the (minimum) distance between any two successive atoms is equal to the triple waist length of the cavity mode, then, the approximate relation between N and the lifetime of the atom-cavity system T, takes the form

$$N \simeq \frac{1}{6}\frac{T}{T_\pi}\varepsilon, \tag{20}$$

where T_π is the required time for a single π Rabi rotation, and ε is a factor which reflects various corrections to our idealized estimate. Such necessary corrections might concern the imperfections in the Rabi and Ramsey pulses, events with two atoms in the same cavity mode, contributions due to noisy channels, etc. Of course, such additional disturbances can lead only to a further decrease of N, the number of atoms in the chain. For the atomic velocity $v = 500$ m/s, as utilized in the microwave cavity experiments, a single π

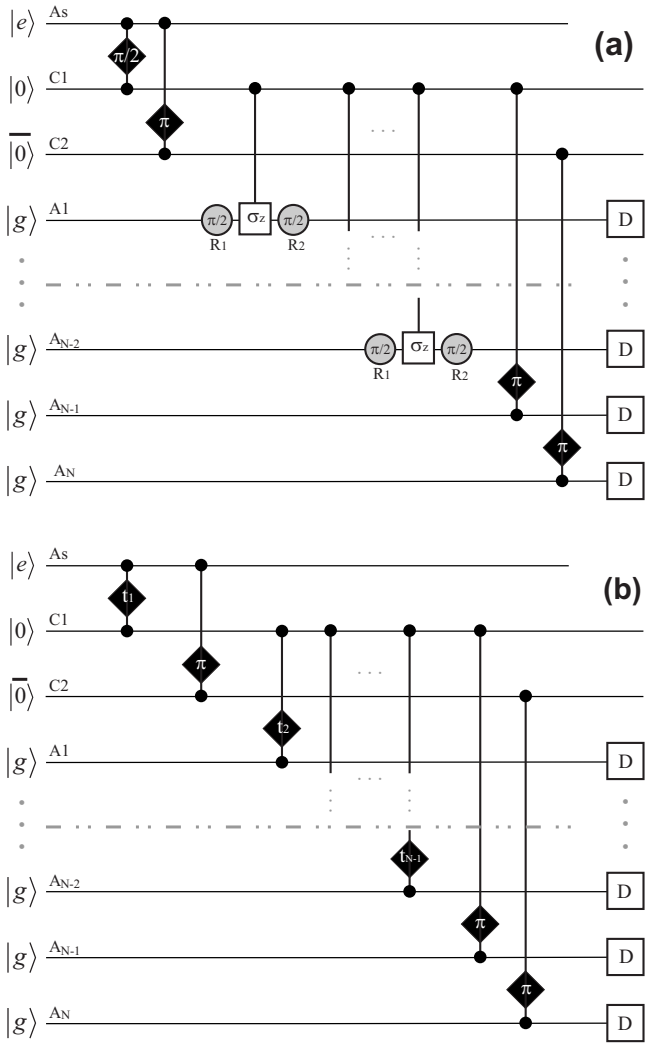

FIG. 4. (a) Quantum circuit for generating a N-partite GHZ state associated with the Rydberg atoms A_1-A_N. (b) The same but for the N-partite W state; see text for further discussions.

Rabi rotation takes about $T_\pi \approx 10\ \mu$s. According to report by Kuhr *et al.*, moreover, the lifetime of the system is bounded only by the radiative lifetime of the atoms $T \simeq 30$ ms (in contrast to the cavity photon storage time $\simeq 120$ ms). Using a conservative estimate of $\varepsilon = 0.2$ in Eq. (20), then, the number of atoms which may pass the cavity within the above lifetime T is given by $N \simeq 100$. In practice, this number must certainly be rescaled in accordance with the physical distances between the atomic source, cavity, and detectors as utilized in a particular experiment.

III. DETECTION OF THE FOUR-PARTITE GHZ AND W STATES

Each scheme for generating experimentally a particular (entangled) multipartite state for a given atom chain should come along with a recipe that enables one to demonstrate that the requested state has indeed been produced. Since, up to the present, we were mainly concerned with the (Rabi and Ramsey) rotations that are necessary in order to achieve the desired state entanglement, not much was said about the detectors D displayed in Figs. 2 and 3. To project the state of a Rydberg atom upon one of its (allowed) levels e, g, or i, a field ionization technique (detector) is applied in the microwave cavity experiments. From the detector signal, as taken for many chains of Rydberg atoms, then the probabilities $P_n(e)$, $P_n(g)$, and $P_n(i)$ are deduced for occupying a particular level. In the experiments, the field ionization of some atom from the chain is often characterized in the literature as longitudinal measurement (experiment).

To better understand why one distinct projective measurement—the transversal measurement—needs to be carried out, let us reconsider the GHZ state (14) from Sec. II A. With probability 1/2, we expect to find the atomic chain A_1-A_4 either in the (basis) state $|i_1,i_2,g_3,e_4\rangle$ or $|g_1,g_2,e_3,g_4\rangle$, and similarly the probability $1/4$ to find the W state (18) in one of the four (basis) states $|g_1,g_2,g_3,e_4\rangle$, $|g_1,g_2,e_3,g_4\rangle$, $|g_1,e_2,g_3,g_4\rangle$, and $|e_1,g_2,g_3,g_4\rangle$, respectively. However, the same probabilities are obtained also for the (uncorrelated) statistical mixture of the corresponding basis states, for instance, the mixed state $[\{1/2,|i_1,i_2,g_3,e_4\rangle\},\{1/2,|g_1,g_2,e_3,g_4\rangle\}]$. Therefore, no (longitudinal) measurement alone is sufficient for proving the nonclassical nature of the correlated atomic chain for the GHZ- or the W-type entanglement, but must be augmented by additional measurements. The same can be seen already from the (Bell) state $\frac{1}{\sqrt{2}}(|\uparrow_1,\downarrow_2\rangle+|\downarrow_1,\uparrow_2\rangle)$ that describes a rotation-invariant spin singlet state of two qubits. As is well known for such a singlet state, we shall find the two spins always in the opposite direction for any choice of the quantization axis of the (projective) measurement. In the literature, this counterintuitive result is known also as Einstein-Rosen-Podolsky (EPR) paradoxon [34], and this freedom in the choice of the quantization axis can therefore be exploited to display the nonclassical correlations of the generated GHZ and W states.

Following the work by Hagley *et al.* [35], let us now adopt the geometrical language of the Bloch sphere in order to introduce a more quantitative description for the projective measurement in the framework of cavity QED. Using the Bloch sphere, any single-qubit state can be represented as a point either on the sphere (pure states) or within the sphere (mixed states). Moreover, the two basis states $|\uparrow_n\rangle$ and $|\downarrow_n\rangle$ are taken along z as the quantization axis that crosses the sphere at the north and south pole, respectively. In this standard representation of the Bloch sphere, the x axis is defined by the vectors $|+_n^x\rangle=\frac{1}{\sqrt{2}}(|\uparrow_n\rangle+|\downarrow_n\rangle)$ and $|-_n^x\rangle=\frac{1}{\sqrt{2}}(|\uparrow_n\rangle-|\downarrow_n\rangle)$, the y axis is defined by vectors $|+_n^y\rangle=\frac{1}{\sqrt{2}}(|\uparrow_n\rangle+i|\downarrow_n\rangle)$ and $|-_n^y\rangle=\frac{1}{\sqrt{2}}(|\uparrow_n\rangle-i|\downarrow_n\rangle)$. In addition, any other axis $\xi(\varphi)$ in the equatorial x-y plane, that forms the angle φ with respect to the x axis, can be characterized by the unit vectors $|+_n^\varphi\rangle=\frac{1}{\sqrt{2}}(|\uparrow_n\rangle+e^{i\varphi}|\downarrow_n\rangle)$ and $|-_n^\varphi\rangle=\frac{1}{\sqrt{2}}(|\uparrow_n\rangle-e^{i\varphi}|\downarrow_n\rangle)$ where, again, the plus and minus signs are chosen to distinguish between positive and negative values along the axis. Recall that the basis states $|\uparrow_n\rangle$ and $|\downarrow_n\rangle$ are related to the two neighbor atomic states $|e_n\rangle$ and $|g_n\rangle$, or $|g_n\rangle$ and $|i_n\rangle$ via expressions (15) or (19) for the four-partite GHZ or W entangled chain of atoms, respectively. By this choice, we thus defined the z axis of the Bloch sphere as pointing along our longitudinal

quantization axis that coincides with the projection measurement performed by the detector.

With this notation, following Hagley *et al.*, we can now explain how one and the same detector (as used for projection along the z axis) can be applied to perform a projection along either the x or $\xi(\varphi)$ (transversal) axes, respectively. If we consider an atom in the superpositions $\frac{1}{\sqrt{2}}(|\uparrow\rangle+|\downarrow\rangle)$ and $\frac{1}{\sqrt{2}}(|\uparrow\rangle-|\downarrow\rangle)$, then a resonant $\pi/2$ Ramsey pulse between the two neighbor levels $|\uparrow\rangle\leftrightarrow|\downarrow\rangle$ implies the transformations

$$\frac{1}{\sqrt{2}}(|\uparrow\rangle+|\downarrow\rangle)\rightarrow|\downarrow\rangle,\quad \frac{1}{\sqrt{2}}(|\uparrow\rangle-|\downarrow\rangle)\rightarrow|\uparrow\rangle. \tag{21}$$

Leaving the Ramsey zone, the atom enters the detector, where it is projected either upon the state $|\downarrow\rangle$ or $|\uparrow\rangle$ corresponding to poles of the Bloch sphere above. The time reversal of the (unitary) transformation (21) thus suggests that a combination of the resonant $\pi/2$ Ramsey pulse followed by a standard (longitudinal) measurement, can be viewed as a projective measurement upon the x axis as given by vectors $|\pm^x\rangle=\frac{1}{\sqrt{2}}(|\uparrow\rangle\pm|\downarrow\rangle)$. Alternately to the resonant Ramsey pulse, if we perform a pulse $R_2(\pi/2,\tilde{\omega})$ with a frequency $\tilde{\omega}$ that is slightly shifted with regard to the atomic transition $(|\uparrow\rangle\leftrightarrow|\downarrow\rangle)$ frequency ω, then a phase difference $\varphi=\tau(\tilde{\omega}-\omega)$ is accumulated by the atomic state during the coherence time τ. Therefore, a combination of a near-resonant Ramsey pulse with a tunable frequency $\tilde{\omega}(\sim\varphi)$ followed by a detection of the atom within the longitudinal basis, is equivalent to a projective measurement upon the $\xi(\varphi)$ axis as described by vectors $|\pm^\varphi\rangle=\frac{1}{\sqrt{2}}(|\uparrow_n\rangle\pm e^{i\varphi}|\downarrow_n\rangle)$. Further details concerning the transversal measurement in cavity QED can be found in by papers by Hagley *et al.*, and Rauschenbeutel *et al.*

To make the above statements clear, let us consider the three-partite GHZ state (10) from Sec. II A and suppose that atom A_1 is projected onto the states $|i_1\rangle$ or $|g_1\rangle$ after it has passed the cavity. For the field modes C_1 and C_2, this projection gives rise to a collapse of the wave packet (10) into one of the (two) Bell states

$$|\Psi^{\pm}_{\text{coll}}\rangle=\frac{1}{\sqrt{2}}(ie^{i\delta 3\pi/\Omega}|0,\bar{1}\rangle\pm|1,\bar{0}\rangle), \tag{22}$$

where the plus sign is associated with the atom in the state $|i_1\rangle$ and the minus sign with $|g_1\rangle$, respectively. These Bell states can be mapped upon the atoms A_2 and A_3 by following the procedure from Sec. II and as seen in Fig. 5(a). After this map, the cavity states are factorized out and the state of the atoms A_2 and A_3 then becomes

$$|\tilde{\Psi}^{\pm}_{\text{coll}}\rangle=\frac{1}{\sqrt{2}}(e^{i\eta}|g_2,e_3\rangle\pm|e_2,g_3\rangle) \tag{23}$$

with $\eta=5\pi\delta/\Omega$. To perform an independent (transversal) measurement on these atoms, we project A_2 upon the x and A_3 upon the $\xi(\varphi)$ axis. This is done by acting with a $R_2(\pi/2,\omega_{e\leftrightarrow g})$ pulse on atom A_2, followed by a projective measurement in the longitudinal basis, together with a near-resonant $R_2(\pi/2,\tilde{\omega})$ pulse upon A_3 as well followed by a projective measurement in the longitudinal basis [see Fig. 5(a)]. Since the latter Ramsey pulse is done with the (near-resonant) frequency $\tilde{\omega}$, the phase difference $\varphi(\sim\tilde{\omega})$ is accumulated during the time τ given by delay between the $R_2(\pi/2,\omega_{e\leftrightarrow g})$ and $R_2(\pi/2,\tilde{\omega})$ pulses.

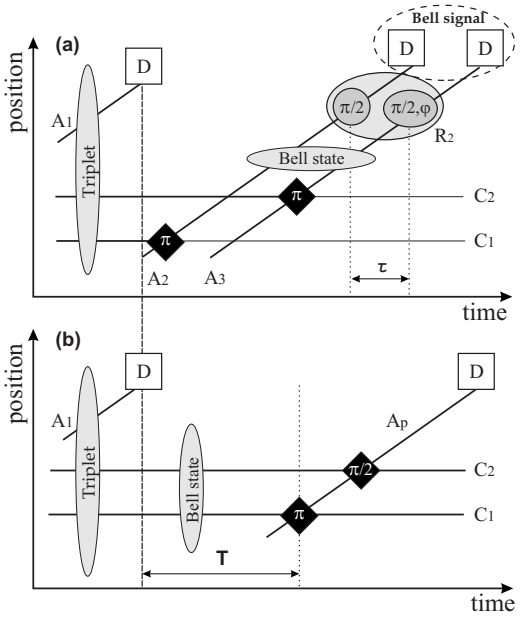

FIG. 5. Sequence (a) displays the basic steps of the transversal measurement for the GHZ state (triplet $A_1-C_1-C_2$) given by expression (10). See the text for explanations. Sequence (b) displays the principle of another type of measurement as applied over the same entangled triplet (10).

The above two sequences: (i) $R_2(\pi/2,\omega_{e\leftrightarrow g})$ acting upon A_2 followed by D and (ii) $R_2(\pi/2,\tilde{\omega})$ acting upon A_3 followed by D, together with the four possible projections $|e_{2,3}\rangle$ and $|g_{2,3}\rangle$ of the atoms A_2 and A_3, give eight outcomes of the measurements with nonzero probability

$$P_{\pm}(e_2,e_3;\varphi)=|(\langle-^x_1|\times\langle-^\varphi_2|)|\tilde{\Psi}^{\pm}_{\text{coll}}\rangle|^2, \tag{24a}$$

$$P_{\pm}(g_2,g_3;\varphi)=|(\langle+^x_1|\times\langle+^\varphi_2|)|\tilde{\Psi}^{\pm}_{\text{coll}}\rangle|^2, \tag{24b}$$

$$P_{\pm}(e_2,g_3;\varphi)=|(\langle-^x_1|\times\langle+^\varphi_2|)|\tilde{\Psi}^{\pm}_{\text{coll}}\rangle|^2, \tag{24c}$$

$$P_{\pm}(g_2,e_3;\varphi)=|(\langle+^x_1|\times\langle-^\varphi_2|)|\tilde{\Psi}^{\pm}_{\text{coll}}\rangle|^2. \tag{24d}$$

Of course, these probabilities depend (parametrically) on the angle φ, that defines the axis for the transversal measurements in the x-y plane, while the subscript $\pm$ refers to the particular state (23) that was obtained after the projection of atom A_1 upon the z axis. The probabilities (24a)–(24d), corresponding to all possible outcomes for A_2 and A_3, are then combined for many instances of one and the same experiment, in order to produce the (so-called) Bell signal

$$I_{\pm}(\varphi)=P_{\pm}(e_2,e_3;\varphi)+P_{\pm}(g_2,g_3;\varphi)-P_{\pm}(e_2,g_3;\varphi)-P_{\pm}(g_2,e_3;\varphi) \tag{25}$$

for any angle φ in the interval $[0,2\pi]$.

For an idealized setup of the experiment, the signal (25) has the form $I_{\pm}(\varphi)=\pm\cos(\varphi+\eta)$ and thus, the observed os-

cillation of the signal as a function of φ, would reveal nonclassical correlations of the Bell states (23). Indeed, the above recipe meets the mentioned request for carrying out an additional measurement upon an independent quantization axis [x and $\xi(\varphi)$ axes in this case], and moreover, since the plus sign is associated with the atom A_1 being in the state $|i_1\rangle$ and the minus sign with $|g_1\rangle$, this technique of transversal measurements enables one to reconstruct quantum correlations of the initial triplet state (10).

Besides varying the angle φ, i.e., the shift in the frequency $\tilde{\omega}$ of the Ramsey pulse $R_2(\pi/2,\tilde{\omega})$ with regard to the atomic transition frequency ω, there is another possibility to perform an independent measurement on the Bell state (22) and which is particularly suitable for bimodal cavities. This technique is based on the delay time T, that is introduced between the creation of the Bell state (22) among the cavity modes C_1-C_2, and the time when the cavity state is probed by one further atom A_p [cf. Fig. 5(b)]. In the latter step, the probe atom A_p prepared in the ground state, first interacts with the cavity mode C_1 for $\Omega t_a=\pi$ and with the mode C_2 for $\Omega t_b=\pi/2$, followed by an projection of A_p in the longitudinal basis. According to Eqs. (6) and (7), for an idealized experiment, this (two-step) sequence produces the probability amplitude to detect A_p in the exited state

$$P_{\pm}(e;T)=\frac{1\pm\cos(\delta T+4\pi\delta/\Omega)}{2}. \tag{26}$$

Again, here the plus sign is associated with the atom A_1 in the state $|i_1\rangle$ and the minus sign with $|g_1\rangle$. An oscillation of the probability amplitude (26) as a function of the delay time T then proves the coherent superposition of the two cavity mode states, and thus, provides us with an entanglement measure similarly to the Bell signal (25) in the previous case. Moreover, the sensibility of this measurement to the sign of the pair (22) enables one also to reconstruct quantum correlations of the initial triplet state (10). Note that the above probing of the cavity modes yields also a nonzero probability to detect A_p in the ground state that fulfills the relation $P_{\pm}(g;T)=P_{\mp}(e;T)$. Therefore, if the probability (26) is chosen in order to reconstruct the state (10), then one should collect only those probabilities during the measurement, for which the probe atom has been detected in its exited state and discard all other events, for which the atom has been detected in its ground state. Further details concerning this technique can be found in the paper by Rauschenbeutel *et al.*

After these brief explanations of the different types of measurement techniques for probing nonclassical correlations, we are prepared to discuss those steps which are necessary for analyzing the four-partite entangled states from Secs. II A and II B.

A. Detection of the four-partite GHZ state

To analyze the four-partite GHZ state from Sec. II A, we shall combine both, the transversal and longitudinal measurement techniques from above. Our goal is to recognize if a (uncorrelated) statistical mixture of the states $|i_1,i_2,g_3,e_4\rangle$ and $|g_1,g_2,e_3,g_4\rangle$ occurs during the experiment, since it leads to the same outcome of the projection (upon the z axis)

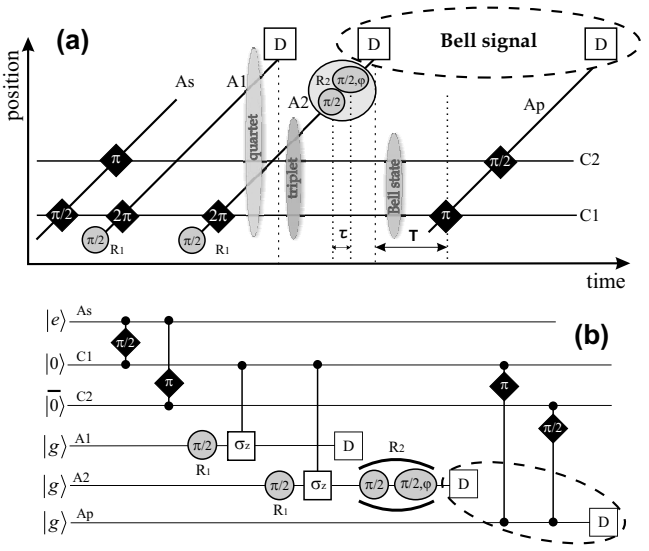

FIG. 6. (a) The temporal sequence for performing transversal measurements on the four-partite GHZ state (quartet $C_1-C_2-A_1-A_2$) given by expression (28). Here the gray shadowed ellipses, triplet and Bell state, correspond to the three-partite GHZ state ($C_1-C_2-A_2$) and two-partite entangled state (C_1-C_2). (b) The quantum circuit that corresponds to the temporal sequence shown in (a).

of individual atoms from the chain as for the entangled GHZ state. Let us start our analysis by considering the three-partite GHZ state (10) from Sec. II A,

$$|\Psi_3\rangle=\frac{1}{\sqrt{2}}(ie^{i\delta 3\pi/\Omega}|+_1^x,0,\bar{1}\rangle-|-_1^x,1,\bar{0}\rangle), \tag{27}$$

where the Bloch sphere notation $|\pm^x\rangle$ along with relations (15) have been used. After the atom A_1 leaves the cavity, atom A_2 prepared in the ground state, is subjected in the first Ramsey zone to the pulse $R_1(\pi/2,\omega_{g\leftrightarrow i})$ and then, while passing the cavity, it interacts with the mode C_1 for $\Omega t_5=2\pi$ as seen in Fig. 6(a). The atom-cavity wave packet thus results into the four-partite GHZ state,

$$|\Psi_5\rangle=\frac{1}{\sqrt{2}}(ie^{i\delta 5\pi/\Omega}|+_1^x,+_2^x,0,\bar{1}\rangle+|-_1^x,-_2^x,1,\bar{0}\rangle). \tag{28}$$

In contrast to Sec. II A, we shall not map the information from the cavity upon some additional atoms but take the (atom-cavity) state (28) itself for performing the transversal measurements.

As seen from Fig. 6(a), the atom A_1 leaves the cavity in either the state $|+_1^x\rangle$ or $|-_1^x\rangle$ and is projected in the detector upon the states $|g_1\rangle$ or $|i_1\rangle$, respectively. This measurement reduces the state (28) to

$$|\Psi_6^{\pm}\rangle=\frac{1}{\sqrt{2}}(ie^{i\delta 5\pi/\Omega}|+_2^x,0,\bar{1}\rangle\pm|-_2^x,1,\bar{0}\rangle) \tag{29}$$

where the plus sign corresponds to the outcome $|g_1\rangle$ and the minus sign to $|i_1\rangle$. Next to A_1, atom A_2 leaves the cavity and is subjected to the pulse $R_2(\pi/2,\omega_{g\leftrightarrow i})$ in the second Ramsey zone, the state (29) thus becomes

$$|\Psi_7^{\pm}\rangle = \frac{1}{\sqrt{2}}(ie^{i\delta 5\pi/\Omega}|i_2,0,\bar{1}\rangle \pm |g_2,1,\bar{0}\rangle). \tag{30}$$

In typical microwave cavity QED experiments, a single $\pi/2$ Ramsey pulse takes about 1 μs-2 μs and implies that the atom A_2 is still inside of the Ramsey plates when the required rotation of the level population has been completed. After a short time delay τ, it is therefore possible to address an additional (near-resonant) $R_2(\pi/2,\tilde{\omega})$ pulse upon A_2 within the same Ramsey zone. Finally, leaving the Ramsey plates, the atom A_2 is projected on either $|i_2\rangle$ or $|g_2\rangle$ state inside the detector [cf. Fig. 6(a)].

As we explained above, the combination of a near-resonant Ramsey pulse $R_2(\pi/2,\tilde{\omega})$ together with the measurement of A_2 in its longitudinal basis is equivalent to a projective measurement upon the $\xi(\varphi)$ axis, where the angle $\varphi=\tau(\tilde{\omega}-\omega_{g\leftrightarrow i})$ is accumulated in the course of the time τ given by delay between the $R_2(\pi/2,\omega_{g\leftrightarrow i})$ and $R_2(\pi/2,\tilde{\omega})$ pulses. After the projection of A_2 upon $|i_2\rangle$ or $|g_2\rangle$, the (two) cavity modes therefore remain either in the state

$$|\Psi_8^{\pm}(i_2;\varphi)\rangle \equiv \sqrt{2}\langle +_2^{\varphi}|\Psi_7^{\pm}\rangle = \frac{1}{\sqrt{2}}(ie^{i(-\varphi+\delta 5\pi/\Omega)}|0,\bar{1}\rangle \pm |1,\bar{0}\rangle) \tag{31a}$$

or

$$|\Psi_8^{\pm}(g_2;\varphi)\rangle \equiv \sqrt{2}\langle -_2^{\varphi}|\Psi_7^{\pm}\rangle = \frac{1}{\sqrt{2}}(ie^{i(-\varphi+\delta 5\pi/\Omega)}|0,\bar{1}\rangle \mp |1,\bar{0}\rangle), \tag{31b}$$

respectively. Although Eq. (31) describe the coherent superposition of the cavity states, they also contain information about the initial four-partite state (28) due to the phase (angle) φ and as well as due to the sign $\pm$.

To reveal the entanglement of (28) due to measurements on the state Eq. (31), we can utilize the last measurement technique from above [see Fig. 5(b)] by introducing a proper time delay T that contributes to the cavity state by means of the energy difference $\hbar\delta T$ between the modes. During this time delay, the free evolution of the cavity state results in the phase shift $e^{i(-\varphi+5\pi\delta/\Omega)} \rightarrow e^{i(T\delta-\varphi+5\pi\delta/\Omega)}$. After this time delay, the probe atom A_p enters the cavity and interacts with the mode C_1 for $\Omega t_a=\pi$ and with C_2 for $\Omega t_b=\pi/2$ as shown in Fig. 6(a). According to Eqs. (6) and (7), the last (two-step) sequence makes the overall state of the cavity and probe atom become either

$$|\Psi_{10}^{\pm}(i_2;\varphi,T)\rangle = \frac{1}{2}[i(1 \mp e^{i(T\delta-\varphi+\theta)})|g_p,0,\bar{1}\rangle + (1 \pm e^{i(T\delta-\varphi+\theta)}) \times |e_p,1,\bar{0}\rangle], \tag{32}$$

if the cavity was initially in the state (31a), or

$$|\Psi_{10}^{\pm}(g_2;\varphi,T)\rangle = \frac{1}{2}[i(1 \pm e^{i(T\delta-\varphi+\theta)})|g_p,0,\bar{1}\rangle + (1 \mp e^{i(T\delta-\varphi+\theta)}) \times |e_p,1,\bar{0}\rangle] \tag{33}$$

for the state (31b), where $\theta=6\pi\delta/\Omega$. Therefore, the four possible projections $|i_2/g_2\rangle$ and $|e_p/g_p\rangle$ of the atoms A_2 and A_p, give the following eight outcomes of the probability amplitudes:

$$P_{\pm}(i_2,g_p;\varphi,T) = |\langle g_p|\Psi_{10}^{\pm}(i_2;\varphi,T)\rangle|^2, \tag{34a}$$

$$P_{\pm}(g_2,e_p;\varphi,T) = |\langle e_p|\Psi_{10}^{\pm}(g_2;\varphi,T)\rangle|^2, \tag{34b}$$

$$P_{\pm}(i_2,e_p;\varphi,T) = |\langle e_p|\Psi_{10}^{\pm}(i_2;\varphi,T)\rangle|^2, \tag{34c}$$

$$P_{\pm}(g_2,g_p;\varphi,T) = |\langle g_p|\Psi_{10}^{\pm}(g_2;\varphi,T)\rangle|^2 \tag{34d}$$

that depend on the angle φ and the time delay T, and where the $\pm$ sign refers again to the outcome $|g_1\rangle$ or $|i_1\rangle$ for the first atom A_1. As before, these probabilities are then combined for many instances of the same temporal sequence, thus producing the correlation signal

$$I_{\pm}(\varphi,T) = P_{\pm}(i_2,g_p;\varphi,T) + P_{\pm}(g_2,e_p;\varphi,T) - P_{\pm}(i_2,e_p;\varphi,T) - P_{\pm}(g_2,g_p;\varphi,T), \tag{35}$$

which is obtained during the experiment. For an idealized setup, this signal takes the form $I_{\pm}(\varphi,T)=\mp\cos(T\delta-\varphi+\theta)$, and where we have the angle $\varphi(\sim\tilde{\omega})$ and the time delay T as two independent parameters that can be varied in order to prove or discard that the desired four-partite state (28) was indeed generated.

B. Detection of the four-partite *W* state

The (N-partite) GHZ and W state are essentially different in that they cannot be transformed into each other under any LOCC operations. For this reason, a quite different (temporal) sequence of transversal measurements must be found in order to prove that the four-partite W state was indeed generated by a given experimental sequence. To develop such a sequence, let us note that the four-partite W state (17) can be cast into the form

$$|\Phi_3\rangle = \frac{1}{\sqrt{2}}\left(\frac{1}{\sqrt{2}}(ie^{i\delta(3\pi/2\Omega+t_2)}|0,\bar{1}\rangle + |1,\bar{0}\rangle)|g_1,g_2\rangle - \frac{1}{\sqrt{2}}(|g_1,e_2\rangle + |e_1,g_2\rangle)|0,\bar{0}\rangle\right), \tag{36}$$

in which we have two types of (two-partite) Bell states: (i) The photonic Bell state in the first line, and (ii) the atomic Bell state in the second line. This representation of the W state therefore suggests a temporal sequence in which the photonic Bell state is coherently isolated and for which the entanglement is shown independent of the atomic part. Indeed, such a (temporal) sequence is shown in Fig. 7(a) and is redrawn as a quantum circuit in Fig. 7(b).

Following Fig. 7, we start from an empty cavity in the state $|0,\bar{0}\rangle$, and make use of an auxiliary source atom A_s to prepare the cavity in the superposition

$$|\Phi_1\rangle = \frac{1}{2}(i|0,\bar{1}\rangle + \sqrt{3}e^{i\delta\pi/\Omega}|1,\bar{0}\rangle). \tag{37}$$

This is done, if the atom first interacts with the mode C_2 for $\Omega t_a=2\arccos(\sqrt{\frac{3}{4}})$ and, thereafter, with the mode C_1 for

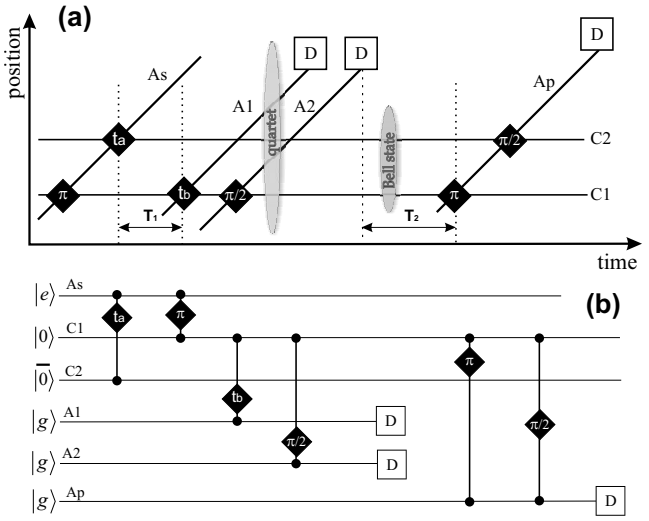

FIG. 7. (a) The temporal sequence for performing transversal measurements on the four-partite W state (quartet $C_1-C_2-A_1-A_2$) given by expression (38). Here the gray shadowed ellipse, Bell state, corresponds to the two-partite entangled state (C_1-C_2). The time intervals t_a and t_b are given in the text. (b) The quantum circuit that corresponds to the temporal sequence shown in (a).

$\Omega t_1=\pi$. Before the atom A_1 enters the cavity, we let the field state (37) evolve freely for the time delay T_1, which leads to the phase shift $e^{i\delta\pi/\Omega}\rightarrow e^{i\delta(T_1+\pi/\Omega)}$. We suppose the atom A_1 to interact with mode C_1 for $\Omega t_b=\arccos(\sqrt{\frac{2}{3}})$ and afterwards A_2 to interact with mode C_1 for $\Omega t_4=\pi/2$ [cf. Fig. 7(a)]. This sequence together then produces the four-partite W state

$$|\Phi_4(T_1)\rangle=\frac{1}{\sqrt{2}}\left[\frac{1}{\sqrt{2}}(i|0,\bar{1}\rangle+e^{i\delta(T_1+3\pi/2\Omega+t_b)}|1,\bar{0}\rangle)|g_1,g_2\rangle-\frac{1}{\sqrt{2}}e^{i\delta(T_1+3\pi/2\Omega+t_b)}(|g_1,e_2\rangle+|e_1,g_2\rangle)|0,\bar{0}\rangle\right] \tag{38}$$

for the atoms A_1,A_2 and the two cavity modes C_1,C_2. When the atoms have left the cavity, they are projected one-by-one in the longitudinal basis inside the detector. We are interested only in those cavity wave packets, for which the atoms A_1,A_2 have been detected in their ground state, and hence, we shall discard all others events right from the beginning. Using such a state-selective procedure, we then know that the state (38) of the atoms is reduced to the photonic Bell state

$$|\Phi_5(T_1)\rangle=\frac{1}{\sqrt{2}}(i|0,\bar{1}\rangle+e^{i\delta(T_1+3\pi/2\Omega+t_b)}|1,\bar{0}\rangle) \tag{39}$$

to which a series of longitudinal measurements can be applied. Notice that the duration of the first time delay T_1 is stored in the phase of (38) and subsequently in the phase of (39). Below, we show how this phase appears as a parameter of the (measured) probability amplitude, and thus, the observed signal provides us with knowledge about the coherence of the initial state (38) before it has been projected upon the ground state $|g_1,g_2\rangle$. At the same time, in order to reveal the coherent superposition of the (entangled) cavity states (39), a second delay time T_2 is introduced in the sequence, before the probe atom A_p enters the cavity [see Fig. 7(a)]. This free time evolution of the cavity field state (39) during the delay T_2 produces the additional phase shift $e^{i\delta(T_1+3\pi/2\Omega+t_b)}\rightarrow e^{i\delta(T_1+T_2+3\pi/2\Omega+t_b)}$, where the durations of delays T_1 and T_2 are manipulated independently.

As in the preceding section, while the probe atom A_p crosses the cavity, it interacts with the mode C_1 for $\Omega t_6=\pi$ and with C_2 for $\Omega t_7=\pi/2$, respectively. These steps together yield the atom-cavity state

$$|\Phi_7(T_1,T_2)\rangle=\frac{1}{2}[i(1-e^{i\delta(T_1+T_2+\theta)})|g_p,0,\bar{1}\rangle+(1+e^{i\delta(T_1+T_2+\theta)})\times|e_p,1,\bar{0}\rangle], \tag{40}$$

with $\theta=[\frac{5\pi}{2}+\arccos(\sqrt{\frac{2}{3}})]/\Omega$. Moreover, the final-state probability to find the probe atom A_p in its excited state is given by

$$P(e_p;T_1,T_2)=\frac{1+\cos[\delta(T_1+T_2+\theta)]}{2}, \tag{41}$$

i.e., by an expression containing two tunable delay times T_1 and T_2 introduced in order to reveal the properties of the initial four-partite W state (38). We note once again that, while T_2 helps to analyze the entanglement of the Bell state (39), T_1 is utilized to control the accuracy of coherence transfer from the state (38) to that of (39).

As before, this (temporal) sequence must be repeated many times in order to reconstruct the final-state probability $P(e_p;T_1,T_2)$ as a function of T_1 and T_2. Note that the state-selective measurements should be here again used as to collect only those probabilities, for which the probe atom has been detected in its exited state. If the four-partite W state from Sec. II B was produced, this probability (distribution) should of course be reasonably close to the predictions in Eq. (41).

IV. SUMMARY AND OUTLOOK

In this work, two schemes are suggested to generate four-partite entangled GHZ and W states within the framework of cavity QED. They are based on the resonant interaction of (a chain of) Rydberg atoms with a bimodal cavity that supports two independent modes of the photon field. In addition, we show how these schemes can be extended toward the generation of N-partite GHZ and W states. To reveal the entanglement of produced states, we also propose the (temporal) sequences of projective measurements and time delays. Using the language of temporal sequences and quantum circuits, a comprehensive description of all necessary manipulations, has been achieved. Our goal is to provide a scheme that can readily be adopted for microwave cavity QED experiments and, in particular, for a forthcoming generation of high-finesse microwave cavities.

Since the experimental reports [24,36,37], the use of bimodal cavities has been found to be an important step toward the manipulation and control of (rather) complex quantum

states. A number of proposals have been made in the literature to exploit further capabilities of bimodal cavities. For instance, in contributions [25–28] the schemes for the engineering of various (multipartite) entangled states between the atomic (chain) and/or photonic qubits have been proposed. In contrast to the present work, however, most of the previous suggestions were not well adopted to the recent design of the cavities, and no satisfactory attempt was made to reveal the nonclassical correlations belonging to the produced states. Another fruitful branch of bimodal cavity applications characterizes the proposal by Zubairy *et al.*, where a bimodal cavity is utilized to realize a quantum phase gate in which the quantum register is represented by the two cavity mode states. Based on this gate, the authors suggested a scheme that enables one to implement Grover's search algorithm by means of a bimodal cavity. We also mention the papers by Queros *et al.*, and Bosco *et al.*, where it has been demonstrated that the coupling of both cavity modes to a common reservoir induces the tunneling of a field state from one cavity mode to another mode of the same cavity device, and thus, opens a way to implement the environment assisted (short-distance) teleporting inside a bimodal cavity. To achieve this goal, i.e., to follow the time evolution of such quantum systems embedded into a reservoir or under the external noise and to analyze different (entanglement or separability) measures, a quantum simulator has been developed recently in our group [38] that can be utilized for such studies in the future.

Finally, let us recall here that all pure (genuine) four-partite entangled states, based on qubits, can be classified into nine classes [39] by using LOCC transformations. Among these classes, we obviously find the four-partite GHZ and *W* states as discussed above. Therefore, an interesting task is to develop schemes that enable one to generate a complete set of genuine entangled states in the framework of cavity QED.

ACKNOWLEDGMENTS

This work was supported by the DFG under Contract No. FR 1251/13.

[1] M. A. Nielsen and I. L. Chuang, *Quantum Computation and Quantum Information* (Cambridge University Press, Cambridge, 2000).
[2] C. H. Bennett and S. J. Wiesner, Phys. Rev. Lett. **69**, 2881 (1992).
[3] A. K. Ekert, Phys. Rev. Lett. **67**, 661 (1991).
[4] L. K. Grover, Phys. Rev. Lett. **79**, 325 (1997).
[5] D. M. Greenberger, M. Horne, and A. Zeilinger, in *Bell's Theorem, Quantum Theory, and Conceptions of the Universe*, edited by M. Kafatos (Kluwer, Dordrecht, 1989), p. 73.
[6] W. Dür, G. Vidal, and J. I. Cirac, Phys. Rev. A **62**, 062314 (2000).
[7] N. D. Mermin, Phys. Rev. Lett. **65**, 1838 (1990).
[8] S. M. Roy and V. Singh, Phys. Rev. Lett. **67**, 2761 (1991).
[9] D. Bouwmeester, J. W. Pan, M. Daniell, H. Weinfurter, and A. Zeilinger, Phys. Rev. Lett. **82**, 1345 (1999); J.-W. Pan *et al.*, Nature (London) **403**, 515 (2000).
[10] M. Eibl, N. Kiesel, M. Bourennane, C. Kurtsiefer, and H. Weinfurter, Phys. Rev. Lett. **92**, 077901 (2004); M. Kiesel *et al.*, J. Mod. Opt. **50**, 1131 (2003).
[11] R. J. Nelson, D. G. Cory, and S. Lloyd, Phys. Rev. A **61**, 022106 (2000).
[12] G. Teklemariam, E. M. Fortunato, M. A. Pravia, Y. Sharf, T. F. Havel, D. G. Cory, A. Bhattaharyya, and J. Hou, Phys. Rev. A **66**, 012309 (2002).
[13] A. Rauschenbeutel *et al.*, Science **288**, 2024 (2000).
[14] The 3-*W* states have not been produced experimentally yet.
[15] C. F. Roos *et al.*, Science **304**, 1478 (2004).
[16] J. M. Raimond, M. Brune, and S. Haroche, Rev. Mod. Phys. **73**, 565 (2001).
[17] S. Haroche and J. M. Raimond, in *Cavity Quantum Electrodynamics*, edited by P. Bergman (Academic, New York, 1994), p. 123.
[18] J.-W. Pan, M. Daniell, S. Gasparoni, G. Weihs, and A. Zeilinger, Phys. Rev. Lett. **86**, 4435 (2001).
[19] C. A. Sackett *et al.*, Nature (London) **404**, 256 (2000).
[20] M. Eibl, S. Gaertner, M. Bourennane, C. Kurtsiefer, M. Zukowski, and H. Weinfurter, Phys. Rev. Lett. **90**, 200403 (2003).
[21] S. Haroche and J. M. Raimond, *Exploring the Quantum: Atoms, Cavities, and Photons* (Oxford University Press, Oxford, 2006).
[22] S. Kuhr *et al.*, Appl. Phys. Lett. **90**, 164101 (2007).
[23] E. T. Jaynes and F. W. Cummings, Proc. IEEE **51**, 89 (1963).
[24] A. Rauschenbeutel, P. Bertet, S. Osnaghi, G. Nogues, M. Brune, J. M. Raimond, and S. Haroche, Phys. Rev. A **64**, 050301(R) (2001).
[25] A. Biswas and G. S. Agarwal, J. Mod. Opt. **51**, 1627 (2004).
[26] M. Ikram and F. Saif, Phys. Rev. A **66**, 014304 (2002).
[27] Y. Zhen-Biao and S. Wan-Jun, Chin. Phys. **16**, 435 (2007).
[28] C. Wildfeuer and D. H. Schiller, Phys. Rev. A **67**, 053801 (2003).
[29] M. S. Zubairy, M. Kim, and M. O. Scully, Phys. Rev. A **68**, 033820 (2003).
[30] I. P. de Queiros, S. Souza, W. B. Cardoso, and N. G. de Almeida, Phys. Rev. A **76**, 034101 (2007).
[31] A. R. Bosco de Magalhaes and M. C. Nemes, Phys. Lett. A **339**, 294 (2005).
[32] D. Gonta and S. Fritzsche, J. Phys. B **41**, 095503 (2008).
[33] In order to be compatible with the Bloch-sphere notation of Sec. III, the fourth qubit should read as $|\uparrow_4\rangle=|e_4\rangle$ and $|\downarrow_4\rangle=|g_4\rangle$. In Sec. II, however, we can safely use the reversed notation from Eqs. (15) in order to represent the 4-GHZ state (14) in the form as it was previously announced in Eq. (3).
[34] A. Einstein, B. Podolsky, and N. Rosen, Phys. Rev. **47**, 777 (1935).

[35] E. Hagley, X. Maitre, G. Nogues, C. Wunderlich, M. Brune, J. M. Raimond, and S. Haroche, Phys. Rev. Lett. **79**, 1 (1997).
[36] Q. A. Turchette, C. J. Hood, W. Lange, H. Mabuchi, and H. J. Kimble, Phys. Rev. Lett. **75**, 4710 (1995).
[37] L. M. Duan and H. J. Kimble, Phys. Rev. Lett. **92**, 127902 (2004).
[38] T. Radtke and S. Fritzsche, Comput. Phys. Commun. **175**, 145 (2006); **176**, 617 (2007).
[39] F. Verstraete, J. Dehaene, B. DeMoor, and H. Verschelde, Phys. Rev. A **65**, 052112 (2002).